Bone Reports 15 (2021) 101129

Contents lists available at ScienceDirect

Bone Reports

journal homepage: www.elsevier.com/locate/bonr

Osteocyte Wnt/β-catenin pathway activation upon mechanical loading is altered in ovariectomized mice

Erica Jackson [a], Nuria Lara-Castillo [a], Mohammed P. Akhter [b], Mark Dallas [a], JoAnna M. Scott [a], Thiagarajan Ganesh [c], Mark L. Johnson [a,*]

[a] UMKC, School of Dentistry, Kansas City, MO 64108, United States of America
[b] Creighton University, Osteoporosis Research Center, Omaha, NE 68122, United States of America
[c] UMKC, School of Computing and Engineering, Kansas City, MO 64110, United States of America

ARTICLE INFO

Keywords:
Mechanical loading
Ovariectomy
β-Catenin signaling
Osteocytes

ABSTRACT

Estrogen levels decline in both sexes with age, but more dramatically in females. Activation of the Wnt/β-catenin signaling pathway is central to the regulation of bone mass accrual and maintenance and in response to mechanical loading. Using the ovariectomized mouse model we examined the effect of estrogen loss on the osteocyte's ability to activate the Wnt/β-catenin pathway following mechanical loading. Female TOPGAL mice underwent ovariectomy (OVX) ($n = 10$) or sham surgery ($n = 10$) at 16 weeks of age. Four weeks post-surgery, a single loading session (global strain of 2200 με for 100 cycles at 2 Hz) was performed on the right forearm with the left as a non-loaded control. Mice ($n = 5$) were sacrificed at 1 or 24 hr post-load. Ulnae were stained for β-catenin activation, femurs were used for μCT and 3-pt bending/biomechanical testing, and tibiae were used for histology analysis and to determine osteocyte lacunar size using SEM and high resolution micro-XCT. A 2.2-fold increase in β-catenin signaling activation was observed 24 hr post-load in the Sham group but did not occur in the OVX group. The OVX group versus control had significant losses ($p < 0.05$) in trabecular BMD (−8%), BV/TV (−35%) and thickness (−23%), along with cortical thickness (−6%) and periosteal perimeter (−4%). The OVX group had significantly higher trabecular bone osteoclast numbers (63%), OCS/BS (77%) and N.OC/BPm (94%) and a significant decrease in osteoblast number (53%), OBS/BS (37%) and N.OB/BPm (40%) compared to the sham group ($p < 0.05$). Cortical bone lacunar number/lacunar volume and bone biomechanical properties did not change between groups. Given that the ulna is a cortical bone loading model and the lack of changes in osteocyte lacunar number/volume in cortical bone, which would alter strains experienced by osteocytes, these data suggest the absence of estrogen resulted in intrinsic changes in the ability of the osteocyte to respond to mechanical load, rather than changes in the biomechanical and architectural properties of bone.

1. Introduction

The skeleton is constantly adapting its mass and architecture to the load environment it experiences. These adaptations are manifested by the interactions of three main bone cells: osteoblasts (bone building cells), osteoclasts (bone resorbing cells) and osteocytes (mature bone cells). The osteocyte is hypothesized to be the main mechanosensory cell in bone (Robling et al., 2008; Lara-Castillo et al., 2015) and is ideally situated in bone to sense mechanical load and translate that load into intracellular biochemical signals. The mechanosensory properties of the osteocyte and its subsequent actions in response to loading signify a well-developed, specialized, and specific process to manage its physiologic needs and adjust bone via multiple signaling cascades and endocrine secretions, both autocrine and paracrine.

One mechanism for how osteocytes respond to load has been proposed that involves the Wnt/β-catenin pathway (Bonewald and Johnson, 2008). In this model, when load is applied to bone, it is hypothesized that prostaglandin E2 (PGE_2) is released from osteocytes. PGE_2 binds to its prostaglandin receptor (EP2/4) and causes Akt activation. Akt can phosphorylate GSK-3β, disassociating from the degradation complex to which β-catenin is bound. Therefore, β-catenin levels rise in the cytoplasm and translocate into the nucleus, where it alters gene expression including an increased production of Wnt expression (Clevers and Nusse, 2012). Wnt is secreted into the extracellular matrix

* Corresponding author.
E-mail address: johnsonmark@umkc.edu (M.L. Johnson).

https://doi.org/10.1016/j.bonr.2021.101129
Received 21 May 2021; Accepted 9 September 2021
Available online 14 September 2021

where it binds to Lrp5/6 and Frizzled (FZ) co-receptors and further activate and amplify the same downstream signaling pathway (Burgers and Williams, 2013; Joiner et al., 2013). Late gene expression results in the production of Axin 2, which inhibits further β-catenin signaling. Recently, we have provided experimental evidence for this model (Lara-Castillo et al., 2015). In those studies, we applied a single load session to the right ulna of the TOPGAL mice to monitor the activation of the Wnt/β-catenin signaling pathway by measuring β-galactosidase activity (product of the LacZ gene driven by the TCF/LEF promoter). The left ulna was used as non-loaded control. We sacrificed the mice at different time points after loading (1, 4, 24, 48 and 72 h). After 1-hour post loading only a subset of osteocytes initially responded to mechanical loading by activating the Wnt/β-catenin signaling pathway. After 4 h post loading, more cells were activated and the peak of osteocyte activation of β-catenin signaling occurs at the 24-hour time point.

Altered Wnt/β-catenin signaling has reported between males and females, including differences in trabecular bone properties of $LRP5^{G171V}$ transgenic high bone mass (HBM) mouse (Dubrow et al., 2007). Major male/female differences have also been reported in bone strength and mass in *SOST* knockout mice (Li et al., 2008) and in mice with a deletion of a single allele of β-catenin in osteocytes (Javaheri et al., 2014). These studies suggest the potential for hormonal differences, specifically regarding estrogen, in the regulation of the Wnt/β-catenin pathway.

The role of estrogen in bone is complex; with both differential roles for estrogen and signaling through its two receptors, ERα and ERβ (Galea et al., 2013), as well as genomic and non-genomic actions (Revankar et al., 2005; Mendelsohn and Karas, 2010). In part, this complexity can be attributed to the different effects of estrogen and ERs on the different cell types in bone (Manolagas, 2013). It has been reported that osteocytes die via apoptosis following estrogen withdrawal (Tomkinson et al., 1997) and that ERα is important in trabecular bone formation in females (Kondoh et al., 2014) and males (Windahl et al., 2013a).

In a study of male rats, low dose estrogen was found to suppress the loading response on the periosteal surface, but had no effect on the endocortical surface (Saxon and Turner, 2006). In a study of ovariectomized female rats, no cortical bone response (formation/loss) was observed following loading (Hagino et al., 1993). Pajamäki et al. (2008) demonstrated that the effects of loading and estrogen on bone structure are independent, yet additive, and also saw no changes in cortical parameters. These studies demonstrate that in both males and females the response to loading is altered by estrogen, but they did not specifically determine the osteocyte's response.

Evidence suggests that ERα is critical for β-catenin nuclear translocation following activation of the Wnt/β-catenin signaling pathway, but this may not require estrogen (Windahl et al., 2013b). A prior study demonstrated that the osteocytes' response to load and estrogen both involve ERα, but only estrogen regulates ERα's cellular concentration (Zaman et al., 2006). This suggests that the bone loss associated with estrogen deficiency is a consequence of the reduction of ERα number/activity that is associated with low estrogen concentration. Another study suggested that activating ERα, using the ER agonist Tamoxifen, increased trabecular bone volume and trabecular thickness in female OVX mice following mechanical loading (Sugiyama et al., 2010).

Given the important role of activation of the Wnt/β-catenin pathway in osteocytes in bone responsiveness to mechanical loading (Robinson et al., 2006; Javaheri et al., 2014; Lara-Castillo et al., 2015), we sought to determine whether estrogen was critical for this pathway activation. In this study we tested the hypothesis that estrogen loss would attenuate activation of osteocyte β-catenin signaling following loading, and if attenuated signaling was due to changes in bone (micro)architectural and/or material properties.

2. Materials and methods

2.1. Animals

At 16 weeks of age, female TOPGAL mice (CD-1 background, purchased from Jackson Laboratories) (DasGupta and Fuchs, 1999) underwent ovariectomy (OVX) ($n = 10$) or a sham ($n = 10$) surgery. Both Sham and OVX surgeries were performed at the Jackson Laboratory and animals were shipped 1-week post-surgery. Four weeks post-surgery, mice were anesthetized with 3.5% isoflurane and a single session of mechanical loading on the right forearm was performed at a global strain of 2200 microstrain (με) for 100 cycles at 2 Hz as previously described (Lara-Castillo et al., 2015). The left forearm of each animal served as a control, non-loaded arm and Sham animals served as control for the OVX group. Five mice per treatment group were sacrificed at 1 hour or 24 hour post-load. All animal procedures are approved by the UMKC Institutional Animal Care and Use Committee (IACUC).

At sacrifice, whole body weight and uterus weight were obtained for each animal, and the ulnae, tibiae, femurs, and uterus were removed. Loaded (right) and non-loaded (left) ulnae were stained for β-galactosidase to assess the TOPGAL gene activation as previously described (Lara-Castillo et al., 2015). Prior to staining, forearms were fixed in ice cold 4% PFA (Cat. No. 43688, Alfa Aesar) for a 60–90 min on ice with gentle rocking, followed by three 5-minute PBS washes. Individual forearms were place in X-gal solution and left in the dark for 36–40 h at 32 °C without shaking, checking periodically for adequate color development. Following staining, forearms were washed with PBS, decalcified, and embedded in paraffin. The right femur was wrapped in phosphate buffered saline (PBS) soaked gauze and stored at −20 °C and used for micro-computed tomography (micro-CT) and biomechanical testing. The right tibia was fixed in 4% PFA, embedded in plastic, and utilized for numerous tests, including histology to determine osteoclast number and surface and osteoblast number by TRAP staining and Von Kossa staining, respectively. The right tibia was also used for backscatter scanning electron microscopy (SEM) and high-resolution microXCT-200 scanning.

2.2. TOPGAL β-catenin quantification

After staining for β-galactosidase, serial 10 μm-thick sections were taken from a region ±1 mm of the midshaft of the ulna. Sections were incubated with primary antibody against Sclerostin (Cat. No. AF1589, R&D Systems) or isotype matched non-immune IgG (Cat. No. AB-108-C, R&D Systems), followed by secondary antibody incubation with Cy3 conjugated donkey anti-goat secondary antibody (Cat. No. 705-165-147, Jackson ImmunoResearch Laboratories, Inc.) and DAPI (Cat. No. D9542-5MG, Sigma-Aldrich). Individual sections were imaged with a Nikon Eclipse E800 light microscope equipped with a high-resolution digital camera at 20× objective for both bright field and fluorescent microscopy. Bright field, Sclerostin and DAPI fluorescent images were analyzed (at the anterior and posterior of the cortex surrounding the medullary cavity) using an in-house MatLab based program that allows for easy and quick quantification of total, sclerostin positive and β-galactosidase positive osteocyte cell numbers. A secondary confirmation of these numbers was performed manually using ImageJ and Microsoft Photo Viewer. A minimum of 32 sections were analyzed per animal, 16 sections for each forearm.

2.3. Micro-CT

Individual right femurs ($n = 10$/group) were imaged using a SkyScan Model 1174 micro-CT scanner using a 0.5 mm aluminum filter, 9.6 μm scanning size, 0.4 rotation step, frame average of 1, 800 μA current and 50 kV voltage. Standard micro-CT measures were taken per ASBMR recommendations (Bouxsein et al., 2010). Reconstruction was carried out with a modified Feldkemp2 algorithm using SkyScan™ NRecon

software. Gaussian smoothing, ring artifact reduction and beam hardening correction were applied. Global thresholds were selected by visual matching with greyscale image and the same global threshold values were applied to all femur samples. The threshold levels for cortical bone were from 55 to 255, and threshold levels for trabecular bone were from 47 to 255.

Trabecular data was collected from a 1 mm region (100 slices) of distal femur proximal to the growth plate and cortical data collected from a 0.5 mm region (50 slices) distal to the 3rd trochanter. 3D and 2D morphometric parameters were calculated for trabecular and cortical bone selected regions of interest using CT Analysis Software. Surface rendering 3D models of trabecular and cortical bone were constructed using CT Vox software.

Three-dimensional analysis was preformed to determine cortical bone volume/total volume (BV/TV), thickness, periosteal, endosteal and total perimeter; trabecular BV/TV, separation, number and thickness; and bone mineral densities (BMD) (cortical and trabecular) (comparison to hydroxyapatite standard).

2.4. Biomechanical testing

Following micro-CT analysis, biomechanical properties of the right femurs (n = 10/group) were obtained using three-point bending to failure testing. Prior to testing, the samples were thawed to room temperature, and kept hydrated during testing. A Bose ElectroForce 3230 mechanical tester with a crosshead displacement rate of 0.1 mm/s was used for all tests. Crosshead displacement and axial load data were recorded using Wintest Software at a rate of 70 Hz. Femurs were oriented in the anterior/posterior direction ex vivo, with a crosshead span of 8.8 mm and the bone centered on the fixture so right and left side overhang was approximately equal. From the 3-pt bending tests, stiffness, ultimate force, moment of inertia, work to failure and Young's Modulus was calculated using realigned micro-CT scans and the BoneJ plug-in for ImageJ.

2.5. Osteoblast and osteoclast assessments

Von Kossa staining was utilized for visualization of osteoblasts on the bone trabecular surface (n = 6/group), using standard staining protocol with McNeal's tetrachrome counterstain (Iwaniec et al., 2008). TRAP staining was utilized for visualization of osteoclasts (multi-nucleated, TRAP positive cells) on bone trabecular surfaces (n = 6/group), following University of Rochester Histopathology Lab protocol (Mundy GR et al., 1991), modified at The University of Missouri - Kansas City (UMKC). All histological sections were analyzed with a light microscope at 20× objective. Six adjacent fields (2 rows of 3, each field = 500 μm^2) were counted 150 μm below the proximal growth plate, to avoid primary spongiosa. Osteomeasure Software was used to obtain osteoblast/osteoclast number, number of osteoblast/osteoclast to bone perimeter, and osteoblast/osteoclast surface to bone surface.

2.6. Backscatter scanning electron microscopy

Following the sectioning of the right tibiae, 3 animals from each group (Sham and OVX), were utilized for backscatter scanning electron microscopy to analyze lacunar area. Specimens were coated with Au—Pd alloy for 60 s. Images were acquired at high vacuum mode. Experimental conditions were accelerating voltage = 15 kV, spot size = 4, working distance = 15 mm, and magnifications of 40× (for reference images) or 300× (for analysis images). Analysis images were taken 1 mm proximal to the end of the medullary cavity, three images anterior and three images posterior. Images were then de-identified prior to analysis for lacunar size via ImageJ. Images were analyzed for particle sizes of 10–250 μm^2, excluding lacunae on edges of images, but including holes. Total lacunae areas were averaged per bone, along with the top 20% largest lacunae per bone, as changes to these lacuna may be substantial (Qing et al., 2012).

2.7. High-resolution microXCT-200

Four Sham and 4 OVX plastic embedded right tibiae that were not utilized for histological sectioning, were utilized for high-resolution microXCT-200 (Xradia/Zeiss Model). Specimens were cut into 300 μm thick sections with a water-cooled diamond saw, 3 mm proximal to the tibia-fibula joint. Measurements were taken on the medial and lateral side of the bone. Measurements obtained were lacunar volume, lacunar-void-volume, and lacunar-void-volume/bone tissue. Mean and standard deviations were determined for each specimen for each measurement, along with top 20% of largest lacunar void volume (Akhter et al., 2017).

2.8. Statistical analysis

An unpaired t-test ($p < 0.05$) was used to compare OVX to Sham groups (when data was normally distributed). Normal data distribution was determined by the Shapiro-Wilk normality test. If data was not normally distributed, a Mann-Whitney U test ($p < 0.05$) was used, reporting medians and interquartile range. Normally distributed data is reported with mean ± standard deviation. Prism Graph Pad was used for all statistical analyses. Body weight, uterus weight, Stiffness, OCS/BS, Lacunar-void volume, and top 20% lacunar void volume were analyzed with Mann-U Whitney test. All other experiments were analyzed by a paired or unpaired t-test.

3. Results

3.1. Body and uterus weight

Body and uterus weight were taken post-sacrifice. While body weight did not change between the two groups (Fig. 1A), the uterus weight was significantly decreased in the OVX group when normalized to body weight ($p < 0.0001$) (Fig. 1B).

3.2. Activation of β-catenin signaling in osteocytes

To determine the activation of the β-catenin signaling following a single session of mechanical loading, β-galactosidase positive cells were counted at 1 hour and 24 hour post-load time points in the anterior and posterior regions of the medullary cavity (Supplemental Fig. 1) as previously described (Lara-Castillo et al., 2015). For both Sham and OVX, β-galactosidase positive cells/DAPI positive cells were calculated for the loaded (L) right ulnae and the non-loaded (NL) left ulnae. Loaded/Non-loaded (L/NL) was calculated to determine the effect of loading. These ratios were then normalized against the Sham 1 hr NL ratio as baseline control. At 1 h, we observed almost no response to loading in β-galactosidase positive cells for both Sham (1.25) and OVX (1.08), and their differences were not significant ($p = 0.31$) (Fig. 2A). For the 24 hour time point (Fig. 2B), we observed a significant increase in β-galactosidase positive osteocytes in the Sham group (2.20) versus the OVX group (0.74) ($p = 0.0079$), with the Sham group showing an increase from its 1 hour number and the OVX group showing a slight decrease from its 1 hour time point. At the 24 hour time point, there was a significant decrease in the number of Sclerostin positive cells in the Sham group (0.6) but no change was observed in the loaded ulnae compared to the non-loaded ulnae in the OVX group (1) ($p = 0.054$) (Fig. 2C).

3.3. Cortical and trabecular properties

Micro-CT was used to analyze potential OVX induced changes in the cortical (n = 10/group) and trabecular (n = 10/group) parameters of the bone. Cortical thickness was the only parameter to show a significant change ($p = 0.04$) between the Sham and OVX groups, with the OVX group having a lower thickness. The periosteal perimeter almost reached

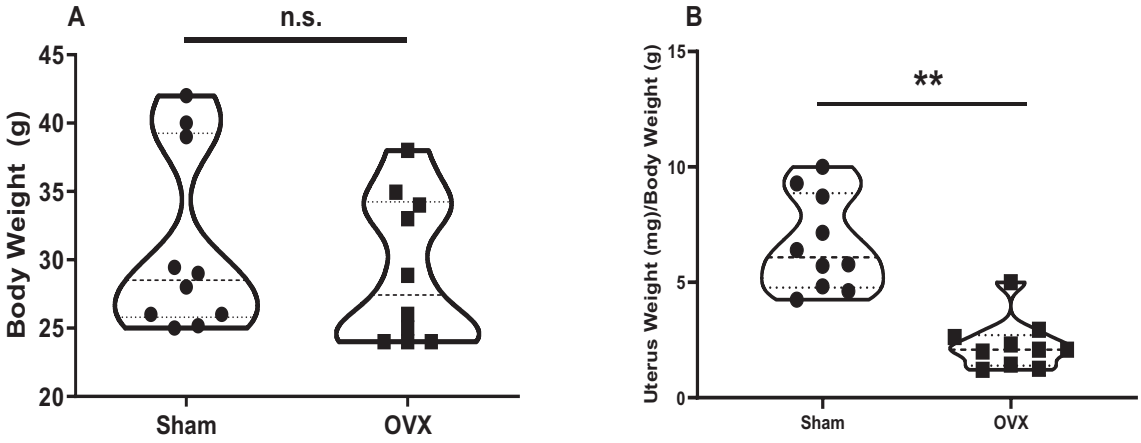

Fig. 1. Uterus weight but not body weight is altered after OVX. Body weight (A) was not significantly different between Sham and OVX, but uterus weight/body weight (B) was significantly decreased in the OVX group. (**$p < 0.0001$; $n = 10$).

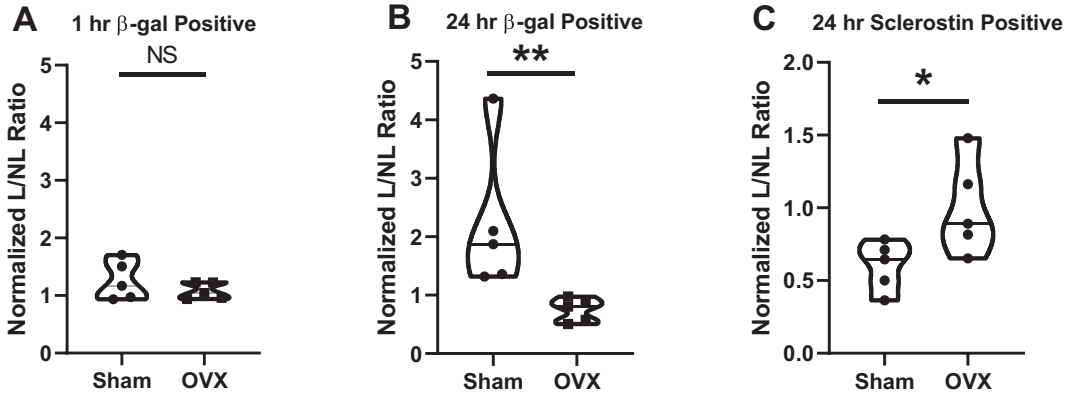

Fig. 2. Effects on OVX on osteocyte β-catenin activation and sclerostin levels in response to loading. (A) normalized ratios of β-galactosidase positive osteocytes in Sham and OVX mice loaded versus non-loaded ulnae 1 hour post-load (B) 24 hour post-load normalized ratios of β-galactosidase positive osteocytes in Sham and OVX mice in loaded versus non-loaded ulnae (C) normalized ratios of sclerostin positive osteocytes in the Sham and OVX loaded group compared to the non-loaded ulna group. (*$p < 0.05$; ** $p < 0.005$, $n = 5$).

a statistically significant decrease ($p = 0.0503$) in the OVX group. All cortical results are shown in Table 1.

Ovariectomy affected trabecular bone as compared to cortical bone. Results of trabecular micro-CT are shown in Table 1. Following micro-CT, three-point bending to failure was conducted on the right femurs.

Table 1
Bone microarchitectural and biomechanical properties.

Architectural properties		Sham ($n = 10$)	OVX ($n = 10$)
Cortical	BMD	1.39 ± 0.09	1.32 ± 0.10
	Ct. Thickness* (mm)	0.19 ± 0.01	0.18 ± 0.12
	Periosteal perimeter (mm)	6.29 ± 0.14	6.02 ± 0.37
	Endosteal perimeter (mm)	3.30 ± 0.14	3.42 ± 0.27
	Total perimeter (mm)	9.59 ± 0.26	9.44 ± 0.54
Trabecular	BMD*	0.96 ± 0.05	0.91 ± 0.042
	BV/TV*	16.77 ± 5.31	10.82 ± 3.73
	Trab thickness* (mm)	0.05 ± 0.01	0.04 ± 0.005
	Trab number	2.96 ± 0.88	2.47 ± 0.72
	Trab separation (mm)	0.25 ± 0.08	0.25 ± 0.05

Biomechanical testing	Sham	OVX
Ultimate load (UL) (N)	15.64 ± 2.43	14.80 ± 2.95
Work to failure (WTF) (mJ)	4.21 ± 1.69	4.19 ± 3.12
Young's modulus (E) (GPa)	4.66 ± 0.83	4.76 ± 1.48
Stiffness (N/mm)	82.32 (65.59, 84.42)	78.7 (54.01, 93.85)

* $p < 0.05$.

Biomechanical testing results are reported in Table 1.

3.4. Osteoblast and osteoclast assessments

Von Kossa staining was used to examine osteoblasts at the trabecular surface of the tibia in the region 150 μm distal to the proximal growth plate. Osteoblasts were counted, along with osteoblast surface and total bone surface. All parameters measured showed a significant decrease in the OVX group as compared to the Sham group. Osteoblast results are reported in Table 2.

TRAP staining was used to examine osteoclasts at the trabecular surface of the tibia in the same region at 150 μm distal to the proximal growth plate. Osteoclasts were counted, along with osteoclast surface and total bone surface. From this, the total number of osteoclasts,

Table 2
Osteoblast and osteoclast properties.

		Sham ($n = 6$)	OVX ($n = 6$)
Osteoblast	Osteoblast number*	17.50 (6.5, 24.5)	7.5 (0, 15.25)
	OBS/BS*	9.07 (5.86, 13.88)	4.49 (0, 8.69)
	N.OB/B.Pm*	6.93 (4.18, 9.71)	2.95 (0, 6.26)
Osteoclast	Osteoclast number*	3 (1, 7)	7.5 (4, 11)
	OCS/BS*	3.59 ± 2.68	6.37 ± 3.70
	N.OC/B.Pm*	1.70 (1.12, 2.57)	3.92 (2.24, 5.27)

* $p < 0.05$.

osteoclasts surface/bone surface (OCS/BS), and number of osteoclasts/bone perimeter (N.OC/B.Pm) were derived. All three parameters showed a significant increase in the OVX group as compared to the Sham group. Osteoclast results are reported in Table 2.

3.5. Backscatter scanning electron microscopy

Lacunar area was measured from backscatter electron microscopy generated images of the right tibia. Images were taken 100 mm proximal to the end of the medullary cavity. Six images were taken per bone, three consecutive images anterior of the medullary cavity and three consecutive images posterior of the medullary cavity ($n = 3$/group). Total lacunar area was counted using ImageJ and top 20% largest lacunar area was also determined, based on findings from Kaya et al. (2017) and Qing et al. (2012). Total lacunar number was consistent between the two groups (Sham = 707; OVX = 684) and total lacunar area was not significantly different ($p = 0.17$). The top 20% largest lacunae were also not significantly different between groups ($p = 0.65$). Supplemental Fig. 2 shows a representative SEM image from a Sham and OVX tibia.

3.6. High-resolution microXCT-200

Plastic embedded right tibiae (4 Sham and 4 OVX) were cut into 300 μm thick sections, 3 mm proximal to the tibia/fibula junction, and the tibiae were imaged for lacunar volume on both the medial and lateral bone sides using high resolution microXCT-200. Lacunar volume, lacunar-void-volume, and lacunar-void-volume/bone tissue for overall samples and the top 20% largest lacunar-void-volumes were not significantly different (Table 3 and Supplemental Fig. 3).

4. Discussion

The osteocyte has been postulated to be the mechanosensory cell of bone (Aarden et al., 1994; Bonewald, 2002; Burr et al., 2002; Ehrlich et al., 2002). Previously we have shown that activation of β-catenin signaling pathway in osteocytes is a requisite for new bone formation (Javaheri et al., 2014) and this activation occurs following in vivo mechanical loading (Lara-Castillo et al., 2015). In this current study, TOPGAL mice were ovariectomized (OVX) or sham operated at 16 weeks of age and used experimentally at 4 weeks post-surgery. Successful OVX was confirmed post-sacrifice by the observed uterine weight decline as previously reported (Sato et al., 2003). Prior to sacrifice, mouse right forearms received a single session of mechanical loading required to activate the Wnt/β-catenin pathway (Robinson et al., 2006; Javaheri et al., 2014; Lara-Castillo et al., 2015; Holguin et al., 2016). We examined osteocyte β-catenin signaling post-loading at 1 h and 24 h and sclerostin expression at 24 hour post-load based on our previous study (Lara-Castillo et al., 2015). We observed the expected increase in β-catenin signaling in osteocytes (~2.2-fold) at 24 hour post-loading, but this increase was not observed in the OVX mice. Sclerostin decreased at 24 hour post-load in the Sham group in agreement with previous reports (Robling et al., 2008; Lara-Castillo et al., 2015), but not in the OVX group. The lack of expected activation of β-catenin and reduction in sclerostin levels suggests the OVX osteocytes were not able to either sense the load (the strain on the osteocytes was below a threshold needed for activation) or respond to the load in the same manner as the Sham group. This leads to the question of what is responsible for the lack of activation in the OVX mice: alterations to the bone biomechanical properties and anatomical structure, on either a whole bone or microarchitecture level, or an intrinsic change to the osteocyte itself in terms of its Wnt/β-catenin signaling pathway?

Table 3
High-resolutions μXCT properties.

	Sham ($n = 4$)	OVX ($n = 4$)
Lacunar number	41,965 ± 8625	36,861 ± 14,767
Lacunar void volume (um^3)	210.9 (139.3–226.0)	228.1 (204.6–231.4)
Top 20% lacunar void volume (um^3)	444.6 (332.9–474.5)	474.4 (447.6–480.8)
Lacunar void volume/bone tissue	0.009 ± 0.002	0.008 ± 0.004

To test bone (micro)architectural properties, micro-CT, high-resolution microXCT-200, backscatter SEM, and 3-point bending were performed. Cortical parameters remained largely unaltered between the OVX and Sham group, with only cortical thickness being significantly lower (6% decrease) in the OVX group. Changes in cortical bone following OVX can be inconsistent (Osterhoff et al., 2016). One study reported no changes to the cortical volume in the mid-shaft region of rat tibia and femur following 4 weeks and 18 weeks post-OVX (Zhang et al., 2007). Another study found an increase in cortical thickness in female rats 8 weeks post-OVX (Rosales Rocabado et al., 2018). The loss of cortical bone identified in the OVX mice may be an effect of the animal model and strain (genetic background). A 2005 study found differences in cortical bone loss following OVX between C57BL/6J (B6), A/J and C3H/HeJ (C3H) strains, with B6 and A/J mice losing cortical area and width 18 weeks post-OVX due to marrow expansion and C3H mice losing cortical width and area at 4 weeks post-OVX due to loss of subperiosteal area (Li et al., 2005). We used TOPGAL mice in this study, which are on the CD-1 genetic background. It seems likely the reduction we observed in cortical thickness in the OVX group would have continued if the study had included longer time periods post-OVX. However, it is not clear if the observed thinner cortex would dramatically alter the load: strain relationship in the OVX bones. Stern et al. (2018) demonstrated that long-term OVX in the rat resulted in a change in the elastic modulus of the perilacunar matrix that changed the strain fields around the osteocyte as predicted by finite element (FE) analysis (2018). Further studies are needed to determine if this might occur in the short-term OVX studies. Additionally, load:strain relationship studies (Mumtaz et al., 2020b) could be performed to determine if this relationship is significantly altered in the OVX mice. At present, the exact strain experienced by each osteocyte on the compression or tensile side of the bone is unknown but could be modeled by finite element analysis (Stern et al., 2018; Kola et al., 2020). Another important caveat to our biomechanical testing and microCT analysis is that those properties were measured in the femur and the loading occurred in the ulna. Based on our recent aging studies in the C57Bl/6 mouse we have shown that there are differences in the biomechanical properties of the ulna, tibia and femur, which may need to be considered when using multiple bones for comparison purpose (Mumtaz et al., 2020a). However, it is reasonable to assume that changes to bone architecture due to OVX would be global. Observed changes to cortical and trabecular bone did not translate to dramatically altered biomechanical properties in the femur, which may be a function of time of sacrifice post-OVX and mouse strain used. Previously it has been shown that C57BL/6J (B6) mice have a slight decrease (7–8%) in the maximum load and stiffness using 4-pt bending at 4 and 8 weeks post-OVX and that decrease almost doubles (14–19%) at 16 weeks post-OVX (Li et al., 2005). Perhaps a longer time span from OVX to sacrifice, i.e. 8 weeks instead of 4 weeks, or utilizing a different murine background would allow for a greater loss of cortical and trabecular bone, leading to differences between the biomechanical properties of the OVX and Sham groups.

Osteocyte lacunae of the tibiae were measured by 2-dimensional analysis through backscatter SEM and by 3-dimensional analysis via high-resolution microXCT following OVX. Previously, it has been shown that osteocytes have the ability to remodel their perilacunar matrix through reversible osteocytic osteolysis, specifically during times of lactation, to maintain blood calcium levels (Qing et al., 2012) and this increase in lacunar size during lactation can lead to reduced tissue-level elastic modulus (Kaya et al., 2017). Although perilacunar remodeling can be seen during lactation times of the reproductive cycle, it may also be a mechanosensitive process (Yee et al., 2019). It has been postulated

that a stiffened perilacunar matrix occurs in estrogen deficient conditions and this leads to a requirement for higher loads (strains) in order to elicit a bone formation response following loading; in the absence of bone formation following loading, bone loss and resorption occur (Frost, 1997). Other studies have also noted changes to rat lacunae with mechanical loading (Ferreyra et al., 2000; Bozal et al., 2001). In human bone tissue that is osteoporotic, there is an increase in hypermineralized osteocyte lacunar number (Carpentier et al., 2012), which may result in the attenuation of mechanical signaling to embedded osteocytes. However, in rat, nanoindentation did not reveal a significant difference in Young's Modulus of the perilacunar area between OVX and Sham groups (Stern et al., 2018).

Backscatter SEM and high-resolution microXCT-200 showed similar results, in that no parameters had significant differences. Osteocyte lacunar number, area, and volume remained unchanged following OVX, suggesting that estrogen does not play a role in osteocytic osteolysis and remodeling at the perilacunar matrix, at least in the short term. However, it cannot be ruled out that estrogen may affect the physiochemical nature of the perilacunar matrix, resulting in alterations to the perceived strain translated to the osteocyte during mechanical loading. Further analysis is needed to determine whether the perilacunar matrix of these animals underwent alterations that lead to a lower strain being sensed by the osteocyte.

It is well established that estrogen deficiency, following menopause or OVX, is associated with bone loss and osteoporosis (Albright et al., 1941). Estrogen is a regulator of bone metabolism in both women and men (Khosla et al., 2008, 2011; Sapir-Koren and Livshits, 2012; Liedert et al., 2020; Dirkes et al., 2021); and estrogen can prevent bone loss following OVX (Lindsay et al., 1976). However, despite the known effects of estrogen in bone mass regulation, it is difficult to define the exact mechanisms or pathways estrogen uses to regulate bone. Since the osteocyte is key to regulating bone remodeling, it is likely that estrogen deficiency first targets the osteocyte, which is then translated to altered control of osteoblast and osteoclast activity and numbers. Osteocyte apoptosis increases following estrogen deficiency in both humans (Tomkinson et al., 1997) and in cortical and trabecular bone of rat tibia (Tomkinson et al., 1998). Treatment with estrogen following OVX prevents osteocyte apoptosis (Tomkinson et al., 1998). Treatment of MLO-Y4 cells with 17β-estradiol prevents etoposide-induced apoptosis by activating the nitric oxide/cGMP/cGMP-dependent protein kinase cascade leading to phosphorylation of Bcl-2 associated death promoter (BAD), a pro-apoptotic protein (Marathe et al., 2012). With a diminished osteocyte population due to estrogen loss, the response to load would be attenuated; however, total osteocyte number was counted in the ulna slices during β-galactosidase activation counting, and no significant differences were observed (not shown), although it is not known whether these cells were alive or not, since a TUNEL assay was not performed. In addition, lacunar number counted during backscatter SEM and high-resolution microXCT-200 was not significantly different either, although it was not determined if these lacunae housed an osteocyte or were empty. This suggests that the regulation of bone turnover following OVX was not due to direct loss of osteocytes but instead due to their lack of response to load and subsequent signaling to osteoclasts and osteoblasts.

Given the established role for activation of β-catenin signaling in response to loading (Robinson et al., 2006; Lara-Castillo et al., 2015; Holguin et al., 2016) and the demonstration that β-catenin is required for new bone formation in response to loading, it seems paradoxical that other reports have shown that estrogen deficiency did not block new bone formation in young male rats (Saxon and Turner, 2006). Two possibilities are plausible. First, the kinetics of activation in the OVX state could be altered so that 24 h, which is peak in control mice, is altered in OVX mice. Second, the activation response may require higher magnitudes of load and/or repeated loading bouts. In a study by Holguin et al. (2016) they found that in young female mice (~5 months) single bouts and multiple bouts of loading produced activation of β-catenin signaling and new bone formation. In 12-month old mice, with multiple bouts of loading, they observed periosteal bone formation, but a lack of activation of β-catenin signaling. Thus, the relationship between activation of β-catenin signaling and bone formation appears to have complexities that we do not yet understand and will require further investigation.

We acknowledge this study has limitations and further research is needed in to fully understand estrogen's role. The rapid growth phase for mice generally ends at 12 weeks of age and mice used in the study were at 16 weeks of age at the time of surgery and endpoints were determined at 20 weeks. Older mice (12 months and 18 months+) would represent a more mature adult and "aged" population, respectively; however, since mice do not experience menopause, OVX would still be necessary to induce estrogen deficiency. Including an OVX + Estrogen group would have allowed identification of which properties were restored with estrogen supplementation. Further studies with finite element modeling, nanoindentation, and strain gauging would be beneficial to assess loading impacts and physiochemical changes at the lacunar level. While the sample size of the OVX and Sham are small ($n = 5$ for each sacrifice time), these numbers are based upon our prior work (Lara-Castillo et al., 2015). Increasing sample sizes may allow for significance in some of the parameters that did not quite reach significance in our current study. Lastly, it would be ideal to study the same bone (ulna) for all properties investigated. However, given the large number of tests performed and the notion that each method requires different processing and, in some of the analysis, destruction of the sample, the number of animal subjects used would increase substantially. As a first approach to these studies, we felt it was more feasible to use different bones for examination, which is a routinely used approach in the field, recognizing that this is a limitation.

In summary, this study demonstrates osteocyte activation of β-catenin signaling in response to *in vivo* loading was significantly attenuated in female mice after 4 weeks post-OVX. We also report significant architectural changes in trabecular, but not cortical, bone. At trabecular bone, the number of osteoclasts increased, while osteoblast numbers decreased. Bone biomechanical properties were unchanged and lacunar number, size and density remained consistent. Although biomechanical and architectural changes were seen at the tibiae and femora, it is likely that the effect of OVX is global and would occur in the ulnae (loaded and non-loaded) as well, with the potential to impact the osteocyte's response to loading. We cannot unequivocally rule out changes to the physiochemical nature of the perilacunar matrix contributing to the lack of activation of β-catenin signaling. However, since the forearm (ulna/radius) loading model primarily loads cortical bone, and cortical bone remained unchanged, we hypothesize that loss of estrogen altered the intrinsic ability of the osteocyte to respond to mechanical loading. These findings have important implications for understanding the reduced response of the skeleton to loading (exercise) in post-menopausal estrogen deficient women.

Declaration of competing interest

None.

Acknowledgements

Portions of this work were submitted to the University of Missouri Kansas City School of Graduate Studies in partial fulfillment of the Ph.D. in Oral and Craniofacial Sciences by Erica Jackson. This work was supported by National Institute on Aging grants PO1 AG039355 and 2PO1 AG039355-06. The authors thank Ms. Yixie Xie for her expert technical assistance and guidance with the histology performed in this study.

Appendix A. Supplementary data

Supplementary data to this article can be found online at https://doi.org/10.1016/j.bonr.2021.101129.

References

Aarden, E.M., Burger, E.H., Nijweide, P.J., 1994. Function of osteocytes in bone. J. Cell. Biochem. 55, 287–299.

Akhter, M.P., Kimmel, D.B., Lappe, J.M., Recker, R.R., 2017. Effect of macroanatomic bone type and estrogen loss on osteocyte lacunar properties in healthy adult women. Calcif. Tissue Int. 100, 619–630.

Albright, F., Smith, P.H., Richardson, A.M., 1941. Postmenopausal osteoporosis: its clinical features. J. Am. Med. Assoc. 116, 2465–2474.

Bonewald, L.F., 2002. Osteocytes: a proposed multifunctional bone cell. J. Musculoskelet. Neuronal Interact. 2, 239–241.

Bonewald, L.F., Johnson, M.L., 2008. Osteocytes, mechanosensing and wnt signaling. Bone 42, 606–615.

Bouxsein, M.L., Boyd, S.K., Christiansen, B.A., Guldberg, R.E., Jepsen, K.J., Müller, R., 2010. Guidelines for assessment of bone microstructure in rodents using micro–computed tomography. J. Bone Miner. Res. 25, 1468–1486.

Bozal, C.B., Fiol, J.A., Ubios, A.M., 2001. Early osteocyte response to bone resorption stimuli. Acta Odontol. Latinoam. 14, 24–29.

Burgers, T.A., Williams, B.O., 2013. Regulation of wnt/beta-catenin signaling within and from osteocytes. Bone 54, 244–249.

Burr, D.B., Robling, A.G., Turner, C.H., 2002. Effects of biomechanical stress on bones in animals. Bone 30, 781–786.

Carpentier, V.T., Wong, J., Yeap, Y., Gan, C., Sutton-Smith, P., Badiei, A., et al., 2012. Increased proportion of hypermineralized osteocyte lacunae in osteoporotic and osteoarthritic human trabecular bone: implications for bone remodeling. Bone 50, 688–694.

Clevers, H., Nusse, R., 2012. Wnt/beta-catenin signaling and disease. Cell 149, 1192–1205.

DasGupta, R., Fuchs, E., 1999. Multiple roles for activated lef/tcf transcription complexes during hair follicle development and differentiation. Development 126, 4557–4568.

Dirkes, R.K., Winn, N.C., Jurrissen, T.J., Lubahn, D.B., Vieira-Potter, V.J., Padilla, J., et al., 2021. Voluntary wheel running partially compensates for the effects of global estrogen receptor-α knockout on cortical bone in young male mice. Int. J. Mol. Sci. 22.

Dubrow, S.A., Hruby, P.M., Akhter, M.P., 2007. Gender specific lrp5 influences on trabecular bone structure and strength. J. Musculoskelet. Neuronal Interact. 7, 166–173.

Ehrlich, P.J., Noble, B.S., Jessop, H.L., Stevens, H.Y., Mosley, J.R., Lanyon, L.E., 2002. The effect of in vivo mechanical loading on estrogen receptor alpha expression in rat ulnar osteocytes. J. Bone Miner. Res. 17, 1646–1655.

Ferreyra, R.S., Ubios, A.M., Gendelman, H., Cabrini, R.L., 2000. Enlargement of periosteocytic lacunae associated to mechanical forces. Acta Odontol. Latinoam. 13, 31–38.

Frost, H.M., 1997. On our age-related bone loss: insights from a new paradigm. J. Bone Miner. Res. 12, 1539–1546.

Galea, G.L., Meakin, L.B., Sugiyama, T., Zebda, N., Sunters, A., Taipaleenmaki, H., et al., 2013. Estrogen receptor alpha mediates proliferation of osteoblastic cells stimulated by estrogen and mechanical strain, but their acute down-regulation of the wnt antagonist sost is mediated by estrogen receptor beta. J. Biol. Chem. 288, 9035–9048.

Hagino, H., Raab, D.M., Kimmel, D.B., Akhter, M.P., Recker, R.R., 1993. Effect of ovariectomy on bone response to in vivo external loading. J. Bone Miner. Res. 8, 347–357.

Holguin, N., Brodt, M.D., Silva, M.J., 2016. Activation of wnt signaling by mechanical loading is impaired in the bone of old mice. J. Bone Miner. Res. 31, 2215–2226.

Iwaniec, U.T., Wronski, T.J., Turner, R.T., 2008. Histological analysis of bone. Methods Mol. Biol. 447, 325–341.

Javaheri, B., Stern, A.R., Lara, N., Dallas, M., Zhao, H., Liu, Y., et al., 2014. Deletion of a single beta-catenin allele in osteocytes abolishes the bone anabolic response to loading. J. Bone Miner. Res. 29, 705–715.

Joiner, D.M., Ke, J., Zhong, Z., Xu, H.E., Williams, B.O., 2013. Lrp5 and lrp6 in development and disease. Trends Endocrinol. Metab. 24, 31–39.

Kaya, S., Basta-Pljakic, J., Seref-Ferlengez, Z., Majeska, R.J., Cardoso, L., Bromage, T.G., et al., 2017. Lactation-induced changes in the volume of osteocyte lacunar-canalicular space alter mechanical properties in cortical bone tissue. J. Bone Miner. Res. 32, 688–697.

Khosla, S., Amin, S., Orwoll, E., 2008. Osteoporosis in men. Endocr. Rev. 29, 441–464.

Khosla, S., Melton, L.J., Riggs, B.L., 2011. The unitary model for estrogen deficiency and the pathogenesis of osteoporosis: is a revision needed? J. Bone Miner. Res. 26, 441–451.

Kola, S.K., Begonia, M.T., Tiede-Lewis, L.M., Laughrey, L.E., Dallas, S.L., Johnson, M.L., et al., 2020. Osteocyte lacunar strain determination using multiscale finite element analysis. Bone Rep. 12, 100277.

Kondoh, S., Inoue, K., Igarashi, K., Sugizaki, H., Shirode-Fukuda, Y., Inoue, E., et al., 2014. Estrogen receptor alpha in osteocytes regulates trabecular bone formation in female mice. Bone 60, 68–77.

Lara-Castillo, N., Kim-Weroha, N.A., Kamel, M.A., Javaheri, B., Ellies, D.L., Krumlauf, R. E., et al., 2015. In vivo mechanical loading rapidly activates beta-catenin signaling in osteocytes through a prostaglandin mediated mechanism. Bone 76, 58–66.

Li, C.Y., Schaffler, M.B., Wolde-Semait, H.T., Hernandez, C.J., Jepsen, K.J., 2005. Genetic background influences cortical bone response to ovariectomy. J. Bone Miner. Res. 20, 2150–2158.

Li, X., Ominsky, M.S., Niu, Q.-T., Sun, N., Daugherty, B., D'Agostin, D., et al., 2008. Targeted deletion of the sclerostin gene in mice results in increased bone formation and bone strength. J. Bone Miner. Res. 23, 860–869.

Liedert, A., Nemitz, C., Haffner-Luntzer, M., Schick, F., Jakob, F., Ignatius, A., 2020. Effects of estrogen receptor and wnt signaling activation on mechanically induced bone formation in a mouse model of postmenopausal bone loss. Int. J. Mol. Sci. 21.

Lindsay, R., Hart, D.M., Aitken, J.M., MacDonald, E.B., Anderson, J.B., Clarke, A.C., 1976. Long-term prevention of postmenopausal osteoporosis by oestrogen. evidence for an increased bone mass after delayed onset of oestrogen treatment. Lancet 1, 1038–1041.

Manolagas, S.C., 2013. Steroids and osteoporosis: the quest for mechanisms. J. Clin. Investig. 123, 1919–1921.

Marathe, N., Rangaswami, H., Zhuang, S., Boss, G.R., Pilz, R.B., 2012. Pro-survival effects of 17β-estradiol on osteocytes are mediated by nitric oxide/cgmp via differential actions of cgmp-dependent protein kinases i and ii. J. Biol. Chem. 287, 978–988.

Mendelsohn, M.E., Karas, R.H., 2010. Rapid progress for non-nuclear estrogen receptor signaling. J. Clin. Invest. 120, 2277–2279.

Mumtaz, H., Dallas, M., Begonia, M., Lara-Castillo, N., Scott, J.M., Johnson, M.L., et al., 2020a. Age-related and sex-specific effects on architectural properties and biomechanical response of the c57bl/6n mouse femur, tibia and ulna. Bone Rep. 12, 100266.

Mumtaz, H., Lara-Castillo, N., Scott, J.M., Begonia, M., Dallas, M., Johnson, M.L., et al., 2020b. Age and gender related differences in load-strain response in c57bl/6 mice. Aging (Albany NY) 12, 24721–24733.

Mundy GR, R.G., Bonewald, L.F., ROC, Oreffo, Boyce, B.F., 1991. Assays for bone formation and bone resorption. In: Barnes, M.J., GH, DSato (Eds.), Methods in Enzymology: Peptide Growth Factors, Part c, Section vii. Academic Press, New York.

Osterhoff, G., Morgan, E.F., Shefelbine, S.J., Karim, L., McNamara, L.M., Augat, P., 2016. Bone mechanical properties and changes with osteoporosis. Injury 47 (Suppl. 2), S11–S20.

Pajamäki, I., Sievänen, H., Kannus, P., Jokihaara, J., Vuohelainen, T., Järvinen, T.L., 2008. Skeletal effects of estrogen and mechanical loading are structurally distinct. Bone 43, 748–757.

Qing, H., Ardeshirpour, L., Pajevic, P.D., Dusevich, V., Jahn, K., Kato, S., et al., 2012. Demonstration of osteocytic perilacunar/canalicular remodeling in mice during lactation. J. Bone Miner. Res. 27, 1018–1029.

Revankar, C.M., Cimino, D.F., Sklar, L.A., Arterburn, J.B., Prossnitz, E.R., 2005. A transmembrane intracellular estrogen receptor mediates rapid cell signaling. Science 307, 1625–1630.

Robinson, J.A., Chatterjee-Kishore, M., Yaworsky, P., Cullen, D.M., Zhao, W., Li, C., et al., 2006. Wnt/b-catenin signaling is a normal physiological response to mechanical loading in bone. J. Biol. Chem. 281, 31720–31728.

Robling, A.G., Niziolek, P.J., Baldridge, L.A., Condon, K.W., Allen, M.R., Alam, I., et al., 2008. Mechanical stimulation of bone in vivo reduces osteocyte expression of sost/sclerostin. J. Biol. Chem. 283, 5866–5875.

Rosales Rocabado, J.M., Kaku, M., Nozaki, K., Ida, T., Kitami, M., Aoyagi, Y., et al., 2018. A multi-factorial analysis of bone morphology and fracture strength of rat femur in response to ovariectomy. J. Orthop. Surg. Res. 13, 318.

Sapir-Koren, R., Livshits, G., 2012. Is interaction between age-dependent decline in mechanical stimulation and osteocyte–estrogen receptor levels the culprit for postmenopausal-impaired bone formation? Osteoporos. Int. 24, 1771–1789.

Sato, T., Fukazawa, Y., Kojima, H., Ohta, Y., Iguchi, T., 2003. Multiple mechanisms are involved in apoptotic cell death in the mouse uterus and vagina after ovariectomy. Reprod. Toxicol. 17, 289–297.

Saxon, L.K., Turner, C.H., 2006. Low-dose estrogen treatment suppresses periosteal bone formation in response to mechanical loading. Bone 39, 1261–1267.

Stern, A.R., Yao, X., Wang, Y., Berhe, A., Dallas, M., Johnson, M.L., et al., 2018. Effect of osteoporosis treatment agents on the cortical bone osteocyte microenvironment in adult estrogen-deficient, osteopenic rats. Bone Rep. 8, 115–124.

Sugiyama, T., Galea, G.L., Lanyon, L.E., Price, J.S., 2010. Mechanical loading-related bone gain is enhanced by tamoxifen but unaffected by fulvestrant in female mice. Endocrinology 151, 5582–5590.

Tomkinson, A., Reeve, J., Shaw, R.W., Noble, B.S., 1997. The death of osteocytes via apoptosis accompanies estrogen withdrawal in human bone. J. Clin. Endocrinol. Metab. 82, 3128–3135.

Tomkinson, A., Gevers, E.F., Wit, J.M., Reeve, J., Noble, B.S., 1998. The role of estrogen in the control of rat osteocyte apoptosis. J. Bone Miner. Res. 13, 1243–1250.

Windahl, S.H., Borjesson, A.E., Farman, H.H., Engdahl, C., Moverare-Skrtic, S., Sjogren, K., et al., 2013a. Estrogen receptor-alpha in osteocytes is important for trabecular bone formation in male mice. Proc. Natl. Acad. Sci. U. S. A. 110, 2294–2299.

Windahl, S.H., Saxon, L., Borjesson, A.E., Lagerquist, M.K., Frenkel, B., Henning, P., et al., 2013b. Estrogen receptor-alpha is required for the osteogenic response to mechanical loading in a ligand-independent manner involving its activation function 1 but not 2. J. Bone Miner. Res. 28, 291–301.

Yee, C.S., Schurman, C.A., White, C.R., Alliston, T., 2019. Investigating osteocytic perilacunar/canalicular remodeling. Curr. Osteoporos. Rep. 17, 157–168.

Zaman, G., Jessop, H.L., Muzylak, M., De Souza, R.L., Pitsillides, A.A., Price, J.S., et al., 2006. Osteocytes use estrogen receptor α to respond to strain but their erα content is regulated by estrogen. J. Bone Miner. Res. 21, 1297–1306.

Zhang, Y., Lai, W.P., Leung, P.C., Wu, C.F., Wong, M.S., 2007. Short- to mid-term effects of ovariectomy on bone turnover, bone mass and bone strength in rats. Biol. Pharm. Bull. 30, 898–903.